Template-Assisted Hydrothermal Synthesis of Li$_2$MnSiO$_4$ as a Cathode Material for Lithium Ion Batteries

Man Xie,[†,‡] Rui Luo,[†] Renjie Chen,*[,†,‡] Feng Wu,[†,‡] Taolin Zhao,[†] Qiuyan Wang,[†,‡] and Li Li[†,‡]

[†]Beijing Key Laboratory of Environmental Science and Engineering, School of Materials Science & Engineering, Beijing Institute of Technology, No. 5 South Zhongguancun Street Haidian District, Beijing 100081, China

[‡]National Development Center of High Technology Green Materials, Beijing 100081, China

ABSTRACT: Lithium manganese silicate (Li$_2$MnSiO$_4$) is an attractive cathode material with a potential capacity above 300 mA h g^{-1} if both lithium ions can be extracted reversibly. Two drawbacks of low electronic conductivity and structural collapse could be overcome by a conductive surface coating and a porous structure. Porous morphology with inner mesopores offers larger surface area and shorter ions diffusion pathways and also buffers the volume changes during lithium insertion and extraction. In this paper, mesoporous Li$_2$MnSiO$_4$ (M-Li$_2$MnSiO$_4$) prepared using MCM-41 as template through a hydrothermal route is compared to a sample of bulk Li$_2$MnSiO$_4$ (B-Li$_2$MnSiO$_4$) using silica as template under the same conditions. Also, in situ carbon coating technique was used to improve the electronic conductivity of M-Li$_2$MnSiO$_4$. The physical properties of these cathode materials were further characterized by SEM, XRD, FTIR, and N$_2$ adsorption−desorption. It is shown that M-Li$_2$MnSiO$_4$ exhibits porous structure with pore sizes distributed in the range 9−12 nm, and when used as cathode electrode material, M-Li$_2$MnSiO$_4$ exhibits enhanced specific discharge capacity of 193 mA h g^{-1} at a constant current of 20 mA g^{-1} compared with 120.1 mA h g^{-1} of B-Li$_2$MnSiO$_4$. This is attributed to the porous structure which allows the electrolyte to penetrate into the particles easily. And carbon-coated M-Li$_2$MnSiO$_4$ shows smaller charge transfer resistance and higher capacity of 217 mA h g^{-1} because carbon coating retains the porous structure and enhances the electrical conductivity.

KEYWORDS: *lithium ion batteries, M-Li$_2$MnSiO$_4$, template-assisted, carbon coating, porous structure*
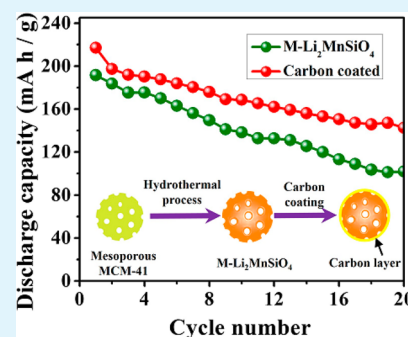
■ INTRODUCTION

Rechargeable lithium ion batteries (LIBs) were originally developed and urgently expanded as high energy power sources not only for portable devices but also for electric vehicles (EVs) and hybrid electric vehicles (HEVs).[1−4] LIBs are also needed in the transportation industry in order to reduce the reliance on fossil fuel and oil.[5,6]

Lithium orthosilicate Li$_2$MSiO$_4$ has attracted considerable attention due to its high theoretical capacity, more than 300 mA h g^{-1} if two lithium ions can be extracted reversibly.[7−11] Additionally, raw materials of lithium orthosilicate are relatively safe, abundant, and low-cost.[12−14] However, the application of Li$_2$MnSiO$_4$ as a cathode material is limited by some drawbacks, such as low electronic conductivity and structural degradation,[7,15,16] resulting in large polarization and poor reversibility with electrochemical cycling.[4,17]

To address these drawbacks, numerous strategies including carbon coating have been developed to enhance the electronic conductivity.[9] Porous structure has also been utilized to reduce the length for Li$^+$ diffusion.[11,12,18,19] Conductive carbon coating has proven to be an effective and simple way to improve the electronic conductivity of polyanion materials. It is generally realized in two ways: ex situ carbon coating and in situ carbon coating.[20] A thin and homogeneous carbon layer can be formed on the surface of particles and contribute to good electrochemical performances.[11]

Mesoporous material with regularly ordered pore arrangement and constant pore diameter from 2 to 10 nm was revealed by the Mobil Corporation Strategy Research Center.[21−23] Since then, numerous research studies have been concentrated on MCM-41. This new family of mesoporous molecular sieves has high specific area (up to 1000 m^2 g^{-1} or higher), a well-defined mesoporous array, and good adsorption properties.[7,22,24,25] These excellent properties endow them with potential applications in catalysis, adsorption, sensors, and LIBs.[26−29] Fabricating a mesoporous architecture with internal pores is a favorable route to buffer the effect of the volume changes during lithium extraction/insertion, and ensure the electrolyte penetration into the materials and thus enlarge the contact area and shorten Li$^+$ extraction/insertion pathways during cycling.[7,30,31] Additionally, template-assisted approaches are widely used for surface modification to create electrostatic or chemical interactions.[2]

Hydrothermal synthesis is one of the routes to prepare pure phase, small, and homogeneous materials with the desired morphology at relatively lower temperature compared to solid state techniques.[10,32] Herein, in this paper, an effective hydrothermal reaction was employed to prepare pure Li$_2$MnSiO$_4$ composites using MCM-41 or common SiO$_2$ as template, which
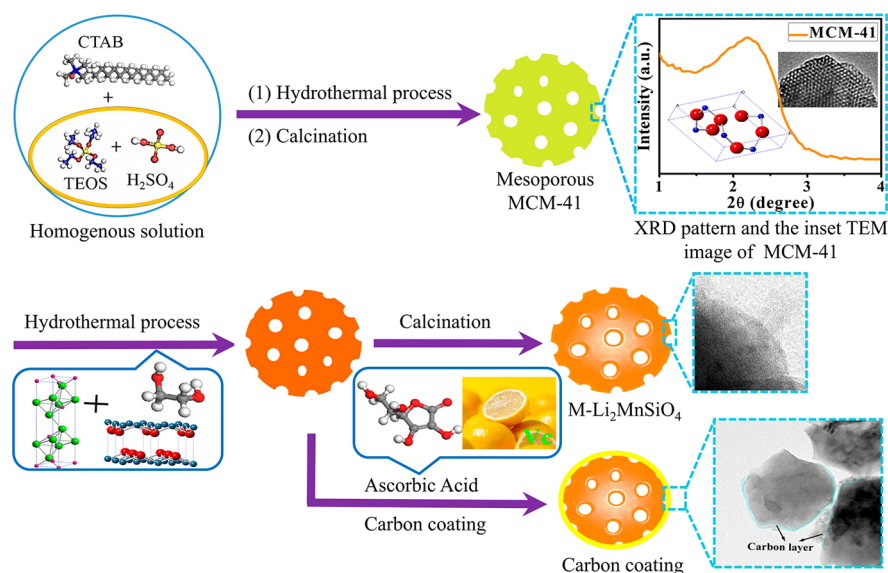
Figure 1. Schematic illustration of preparation of mesoporous MCM-41 and the Li_2MnSiO_4 samples.

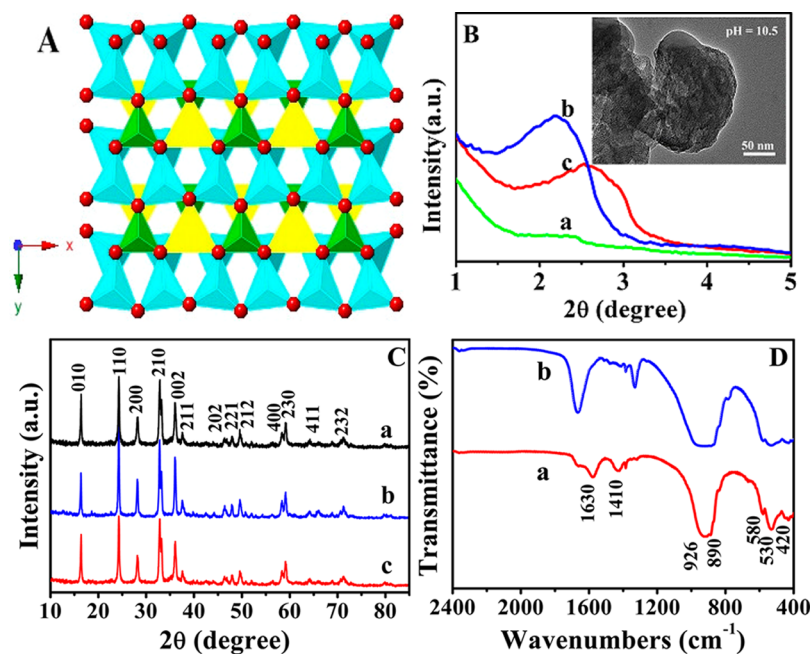**Figure 2.** (A) Projections of crystal structure of Li_2MnSiO_4 along the $[001]$ (z) directions, with orthorhombic ($Pmn2_1$) structure where MnO_4 (marked light yellow) and SiO_4 (marked green) tetrahedra all aligned in the same direction. Oxygen atoms are denoted by red balls, and LiO_4 are colored in cyan. (B) XRD patterns of mesoporous MCM-41 template at different pH conditions (a, pH = 9.5; b, pH = 10.5; c, pH = 11.5). (C) XRD patterns of B-Li_2MnSiO_4 (black line), M-Li_2MnSiO_4/C (blue line), and carbon-coated M-Li_2MnSiO_4/C (red line). (D) FT-IR transmittance spectrum for M-Li_2MnSiO_4 (a, before cycling test; b, after 10 cycles).

were called M-Li_2MnSiO_4 and B-Li_2MnSiO_4, respectively. Additionally, the impacts of carbon coating on the structural, morphological, and electrochemical characteristics of Li_2MnSiO_4 were also investigated in our study. As a cathode material for lithium ion battery, the porous cathode material significantly enhanced the specific capacity, benefiting the design of electrode materials with high surface area for the lithium ion battery field.

■ EXPERIMENTAL SECTION

Preparation processes of MCM-41 template and Li_2MnSiO_4 nanoparticles in this study were performed through a hydrothermal method,[33,34] and the synthetic routes are schematically illustrated in Figure 1. In a typical procedure, a mixture of TEOS (tetraethylortho-

silicate, $Si(OC_2H_5)_4$) and H_2SO_4 solution was stirred at room temperature until it was clear. CTAB (cetyltrimethyl ammonium bromide) was added to the above mixture under vigorous stirring. After that, NaOH solution was dropwise added into the above solution in order to adjust the pH value to 9−12. The homogeneous solution was transferred into hydrothermal reactor and then was heated at 100 °C for 48 h in an oven. Subsequently, the resultant solution was filtered, washed repeatedly with deionized water, and dried overnight at 100 °C. Finally, the dried sample was calcined at 550 °C for 7 h to obtain the MCM-41 powder.

Stoichiometric amounts of lithium hydroxide ($LiOH \cdot H_2O$) and mesoporous MCM-41 were added in deionized water under vigorous stirring to form homogeneous dispersion. Then, the solution containing stoichiometric manganese chloride ($MnCl_2 \cdot 4H_2O$) dissolved in

hexanediol was added into the above homogeneous dispersion. Afterward, the resultant mixture was stirred vigorously for several hours and transferred to an oven at 150 °C for 48 h, and then dried at 60 °C overnight to obtain the precursor powder. As for in situ carbon-coated M-Li$_2$MnSiO$_4$, the obtained precursor powder was thoroughly ground with ascorbic acid to form a homogeneous carbon layer; the content of carbon source was mixed with precursor powder at a weight ratio of 1.5:10. Finally, the carbon-mixed powder was heated in Ar atmosphere at 750 °C in a closed tube furnace. For comparison, bulk sample was also prepared with similar procedure using fumed silica as template.

The morphologies and particle size of the as-synthesized Li$_2$MnSiO$_4$ composites were examined by FE-SEM (field emission scanning electron microscopy, Zeiss, S-3500N) and TEM (transmission electron microscopy, JEOL-2010). XRD was performed on a diffractometer (Rigaku Ultima IV) using Cu Kα radiation. FT-IR spectra were obtained on an infrared spectrometer (NEXUS-670). For fabrication of the cathode electrodes, 80 wt % of the as-prepared cathode material, 10 wt % of super P conductive carbon black, and 10 wt % polyvinylidene fluorid (PVDF) as binder in N-methylpyrrolidinone (NMP) were ground to obtain the slurry, which is coated onto aluminum foil. The electrodes were dried overnight at 120 °C in an oven. Electrochemical measurements were carried out by using CR2025 type coin cells. The as-prepared electrodes were used as cathodes and lithium metal as an anode, while the electrolyte was 1 M LiPF$_6$ dissolved in a mixture of ethylene carbonate−diethyl carbonate (EC/DEC = 1:1 v/v). All cells were tested in a voltage range 1.5−4.8 V at 0.1 C rate. The electrochemical impedance spectroscopy (EIS) measurements were performed on an electrochemical workstation (CHI 604D).

■ RESULTS AND DISCUSSION

The structures of the MCM-41 template and the Li$_2$MnSiO$_4$ samples are shown in Figure 2. The low angle XRD patterns of MCM-41 from 1° to 5° are also shown in Figure 2B, and inset is the corresponding TEM image of MCM-41 synthesized at pH = 10.5. MCM-41 synthesized at pH = 10.5 has a strong peak at 2θ = 2°−3°, corresponding to (100) reflection of highly ordered mesoporous MCM-41 structure. The value of d_{100} is calculated to be 4.033 nm by the Braggs law ($2d \sin \theta = n\lambda$), as seen in Table 1.

Table 1. Structure Properties of the As-Synthesized MCM-41 at pH = 10.5

sample	pH	$a_0{}^a$ (nm)	$d_{100}{}^b$ (nm)	$D_p{}^c$ (nm)	S_{BET} (m^2 g^{-1})	V (cm^3 g^{-1})^c
MCM-41	10.5	4.657	4.033	3.537	839.9	0.734

^{a}Unit cell parameter $a_0 = 2d_{100}/3^{1/2}$. ^{b}Interplanar crystal distance along [100] direction. ^{c}Pore diameter (D_p) and pore volume (V) determined by N$_2$ adsorption−desorption.

As for the other two samples prepared at pH = 11.5 and 9.5, the (100) peak is lower and cannot be observed, due to the less ordered structure. In general, the XRD patterns of MCM-41 are in good agreement with earlier reports.[22,24]

Crystal structures of the as-prepared Li$_2$MnSiO$_4$ composites were analyzed with XRD patterns shown in Figure 2C. As can be seen from the XRD results, all three samples demonstrate similar XRD patterns, which are assigned to the Li$_3$PO$_4$ phase[35] and match well to that of the orthorhombic crystal structure with a space group of Pmn2$_1$. Generally, under our experimental conditions, there are no noticeable additional peaks attributed to impurity phases as reported in many literature studies, such as MnO and Li$_2$SiO$_3$, indicating that the Li$_2$MnSiO$_4$ samples were successfully prepared on the basis of both mesoporous MCM-41 and silica powder. In the case of using a MCM-41 template, the

diffraction peaks of Li$_2$MnSiO$_4$ become sharper, indicating a higher degree of crystallinity. As for carbon-coated sample, the diffraction peaks show a lower intensity indicating that a higher content of carbon leads to lower crystallinity, which is in good agreement with an earlier report.[20]

The FT-IR spectrum can provide supplementary evidence for the structure of M-Li$_2$MnSiO$_4$. Figure 2D shows the bands corresponding to the internal vibrations of the silicate anions in the range 400−2400 cm^{-1}. The positions of 890, 926, and 530 cm^{-1} are characteristic absorption peaks of [SiO$_4$]. The peaks at 890 and 926 cm^{-1} exhibit v_1 and v_3 mode of Si−O bonds, while the peaks at 530 and 580 cm^{-1} are assigned to v_4 vibrations.[32] The low frequency peaks at 420 cm^{-1} perhaps indicate the motion of lithium ions. After 10 cycles, the characteristic adsorption peaks of [SiO$_4$] undergo drastic changes. The peaks at 890 and 926 cm^{-1} merge into a broad peak, and slightly shift to the high frequency. A new adsorption band emerges during cycling around 790 cm^{-1}, which may be attributed to the bending vibration of Si−O−Si bonds in some [SiO$_3$] group due to the reducible reaction condition.

The morphologies of as-prepared products were characterized using scanning electron microscopy (SEM). As can be seen from Figure 3, the as-prepared B-Li$_2$MnSiO$_4$ particles (Figure 3A,a) and M-Li$_2$MnSiO$_4$ particles (Figure 3B,b) are well-distributed secondary particles composed of uniform round primary particles. The SEM micrographs of the carbon-coated M-Li$_2$MnSiO$_4$ (Figure 3C,c) show that materials are composed of individual particles around 100 nm in size with a clearly visible carbon coating layer. This carbon film, indicating the formation of surface secondary phase, could reduce the surface energy of the material, suppress the particle growth during heat treatment, and therefore shorten ion pathways and effectively enhance electronic conductivity.[9,20] Carbon content was appropriately 5.919 wt % determined by thermal gravimetric analysis.

The porous size distribution and Brunauer−Emmett−Teller (BET) surface area of the MCM-41 template and Li$_2$MnSiO$_4$ composites were further studied by the N$_2$ adsorption−desorption analysis (Figure 4A,B). In this work the appropriate synthetic pH of MCM-41 is 10.5, and the corresponding structure properties are listed in Table 1. The porous MCM-41 template exhibits an ideal mesoporous structure as the adsorption−desorption isotherm of the MCM-41 template appears to be a type-IV curve[2,29] (Figure 4A). Also, pore sizes of MCM-41 are well-distributed between 3 and 6 nm. For Li$_2$MnSiO$_4$ composites, the adsorption−desorption isotherm of the M-Li$_2$MnSiO$_4$ particles is quite similar to that of the MCM-41 template. However, the pore size distribution plot of M-Li$_2$MnSiO$_4$ particles shows a larger range 9−20 nm, which can be explained by the destroyed mesoporous structure of MCM-41 during synthetic process. Thus, M-Li$_2$MnSiO$_4$ particles show a BET specific surface area of only 65 m^2 g^{-1}, smaller than the specific surface area of MCM-41 template which is calculated to be 839 m^2 g^{-1}. For comparison, the adsorption−desorption isotherm of the B−Li$_2$MnSiO$_4$ composite (Figure 4B) does not exhibit a typical adsorption hysteresis loop. Nevertheless, the porous structure of M-Li$_2$MnSiO$_4$ particles is beneficial to the penetration of electrolyte to promote the lithium ion transportation.

The electrochemical properties of the corresponding cathode materials were evaluated by galvanostatic charge−discharge cycling and electrochemical impedance spectroscopy (EIS). Figure 5A shows the charge−discharge profiles for initial cycle of as-prepared electrodes in constant current between 1.5 and 4.8 V.
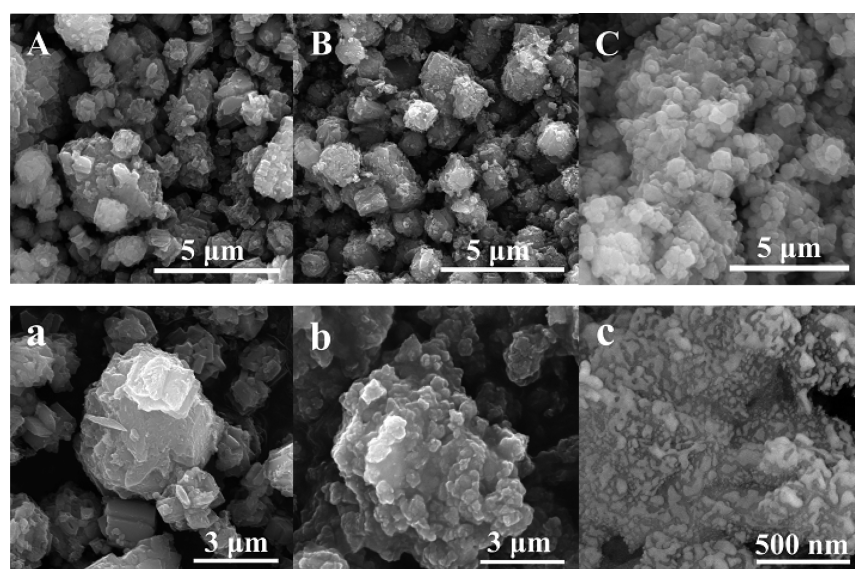
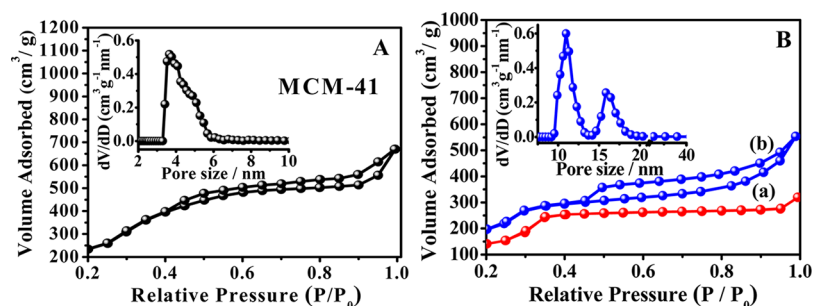**Figure 3.** SEM images of B-Li$_2$MnSiO$_4$ (A, a), M-Li$_2$MnSiO$_4$ (B, b), and carbon-coated M-Li$_2$MnSiO$_4$ (C, c).

Figure 4. N$_2$ adsorption−desorption isotherm plots of (A) mesoporous MCM-41 template and (B) Li$_2$MnSiO$_4$ samples (a, B-Li$_2$MnSiO$_4$; b, M-Li$_2$MnSiO$_4$). Inset shows the corresponding pore size distribution.
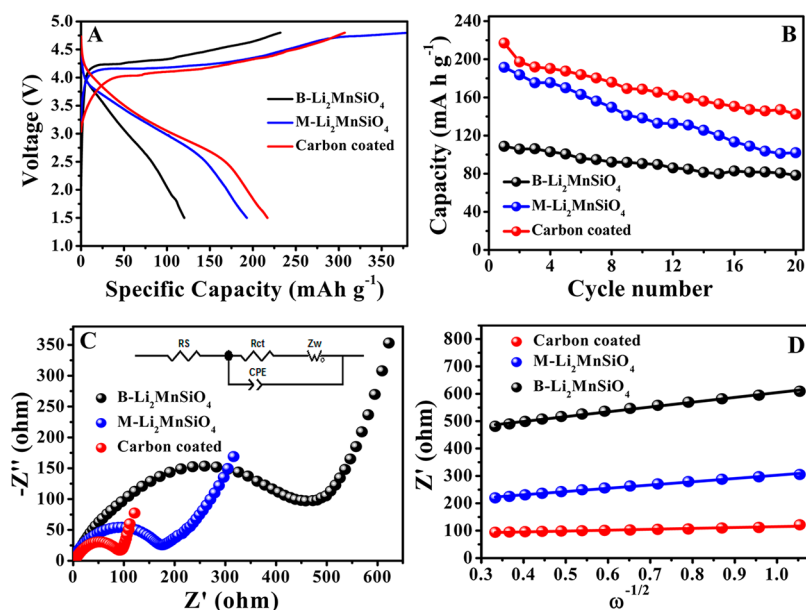

Figure 5. Electrochemical properties: (A) initial charge and discharge profiles, (B) cycling performance. Nyquist plots of (C) B-Li$_2$MnSiO$_4$ (black), M-Li$_2$MnSiO$_4$ (blue), and (D) carbon-coated M-Li$_2$MnSiO$_4$ (red).

The initial discharge capacity of the M-Li$_2$MnSiO$_4$ electrode is about 190 mA h g^{-1}, which is higher than that of the B-Li$_2$MnSiO$_4$ (about 120 mA h g^{-1}). This can be understood as

porous structure cathode material M-Li$_2$MnSiO$_4$ affords increased surface area and a shorter diffusion length for Li$^+$ at a

constant process. Additionally, the carbon-coated electrode shows the highest initial discharge capacity of 217 mA h g^{-1}.

The cycling performances (Figure 5B) of as-prepared electrodes were carried out at a constant current of 20 mA g^{-1}. The discharge capacities of the three materials all decrease gradually during cycling but undergo different fading rates. Discharge capacities of M-Li$_2$MnSiO$_4$ decrease rapidly during cycling, while the carbon-coated sample shows more stabilized capacity retention. Additional measurements such as the change in charge regime[7] as well as the optimization of the synthesis conditions likely lead to a recovery of the lost capacity and improved capacity retention.

EIS tests were carried out for a further understanding of the electrochemical kinetic process of as-prepared electrodes during charge−discharge process. Figure 5C shows the Nyquist plots of the B-Li$_2$MnSiO$_4$, M-Li$_2$MnSiO$_4$, and carbon-coated M-Li$_2$MnSiO$_4$ composites. Each Nyquist plot combines a depressed semicircle in the high frequency region which is ascribed to the charge transfer process and a linear plot in the low frequency region representing typical behavior.[2,10,18] The diameter of the semicircle in the high frequency region is equal to R_{ct} (charge transfer resistance). The M-Li$_2$MnSiO$_4$ electrode exhibits a charge transfer resistance of 175 Ω, smaller than that of B-Li$_2$MnSiO$_4$, indicating a facile Li$^+$ charge transfer and then good electrochemical performance. This can be attributed to the porous structure of M-Li$_2$MnSiO$_4$ and then the shorter diffusion paths. Notably, carbon-coated electrode enjoys the smallest R_{ct} of less than 100 Ω, implying that carbon coating can greatly improve the electronic conductivity. Figure 5D displays the relationship between Z' and the reciprocal square root of the frequency $(\omega^{-1/2})$ in the low frequency region, and the slope of the straight line is σ. The Li$^+$ diffusion coefficients calculated from the EIS results are summarized in Table 2. As shown in Table 2,

Table 2. Fitting Parameter Obtained from the Electrochemical Impedance Spectroscopy (EIS) Data to the Equivalent Circuits Shown in Figure 5C

sample	σ	Li$^+$ diffusion coefficient (cm^2 S^{-1})	transfer resistance (Ω)
B-Li$_2$MnSiO$_4$	175.708	6.8×10^{-16}	458
M-Li$_2$MnSiO$_4$	119.29	1.5×10^{-15}	176
carbon-coated	32.4091	2.0×10^{-14}	92

the calculated diffusion coefficients of lithium ion (D_{Li}+) of the three samples are 6.8×10^{-16}, 1.5×10^{-15}, and 2.0×10^{-14} cm^2 S^{-1}. Compared with the B-Li$_2$MnSiO$_4$ and M-Li$_2$MnSiO$_4$ electrodes, the carbon-coated one shows larger Li$^+$ diffusion coefficients. In summary, the enhanced electronic conductivity and ionic conductivity lead to improved reaction kinetics and thus excellent charge−discharge performances.

CONCLUSIONS

In this study, Li$_2$MnSiO$_4$ cathode particles are synthesized through an effective template-assisted hydrothermal route. The as-prepared M-Li$_2$MnSiO$_4$ sample with porous architecture shows substantially higher specific charge−discharge capacity of 193 mA h g^{-1} than that of B-Li$_2$MnSiO$_4$. The outstanding electrochemical performance is ascribed to the unique pore structure and improved specific contact area, which leads to better diffusion of electrolyte and shorter ion diffusion pathways. After carbon coating, the homogeneous carbon layer greatly contributes to high electronic conductivity, which thus leads to

smaller charge transfer resistance of less than 100 Ω and better charge−discharge performances of the cathode material. In our report, fabricating porous structure and carbon coating strategy are effective routes for synthesizing Li$_2$MnSiO$_4$ cathode materials with high performance. Our results suggested a feasible way for production of high surface area electrode materials in energy storage applications.

AUTHOR INFORMATION

Corresponding Author

*E-mail: chenrj@bit.edu.cn.

Notes

The authors declare no competing financial interest.

REFERENCES

(1) Armand, M.; Tarascon, J. M. Building Better Batteries. *Nature* **2008**, *451*, 652−657.

(2) Kim, S. J.; Suk, J.; Yun, Y. J.; Jung, H. K.; Choi, S. Mesoporous Silica-Assisted Carbon Free Li$_2$MnSiO$_4$ Cathode Nanoparticles for High Capacity Li Rechargeable Batteries. *Phys. Chem. Chem. Phys.* **2014**, *16*, 2085−2089.

(3) Zhang, C.; Chen, Z.; Zeng, Y.; Zhang, Z.; Li, J. Insights into Changes of Lattice and Electronic Structure Associated with Electrochemistry of Li$_2$CoSiO$_4$ Polymorphs. *J. Phys. Chem. C* **2014**, *118*, 7351−7356.

(4) Deng, C.; Zhang, S.; Fu, B. L.; Yang, S. Y.; Ma, L. Characterization of Li$_2$MnSiO$_4$ and Li$_2$FeSiO$_4$ Cathode Materials Synthesized via a Citric Acid Assisted Sol−Gel Method. *Mater. Chem. Phys.* **2010**, *120*, 14−17.

(5) Ellis, B. L.; Nazar, L. F. Sodium and Sodium-Ion Energy Storage Batteries. *Curr. Opin. Solid State Mater. Sci.* **2012**, *16*, 168−177.

(6) Simon, P.; Gogotsi, Y.; Dunn, B. Where Do Batteries End and Supercapacitors Begin? *Science* **2014**, *343*, 1210−1211.

(7) Gummow, R. J.; He, Y. Mesoporous Manganese-Deficient Lithium Manganese Silicate Cathodes for Lithium-Ion Batteries. *RSC Adv.* **2014**, *4*, 11580−11584.

(8) Wang, M.; Yang, M.; Ma, L.; Shen, X.; Zhang, X. Structural Evolution and Electrochemical Performance of Li$_2$MnSiO$_4$/C Nanocomposite as Cathode Material for Li-Ion Batteries. *J. Nanomater.* **2014**, *4*, 1−6.

(9) Gummow, R. J.; Han, G.; Sharma, N.; He, Y. Li$_2$MnSiO$_4$ Cathodes Modified by Phosphorous Substitution and the Structural Consequences. *Solid State Ionics* **2014**, *259*, 29−39.

(10) Jiang, X.; Xu, H.; Liu, J.; Qian, Y. Hydrothermal Synthesis of the Li$_2$MnSiO$_4$/C Nanocomposite as a Cathode Material for Lithium-Ion Batteries. *Mater. Lett.* **2013**, *113*, 9−12.

(11) Sun, D.; Wang, H.; Ding, P.; Zhou, N.; Huang, X.; Tan, S.; Tang, Y. In-Situ Synthesis of Carbon Coated Li$_2$MnSiO$_4$ Nanoparticles with High Rate Performance. *J. Power Sources* **2013**, *242*, 865−871.

(12) Liu, J.; Xu, H.; Jiang, X.; Yang, J.; Qian, Y. Facile Solid-State Synthesis of Li$_2$MnSiO$_4$/C Nanocomposite as a Superior Cathode with a Long Cycle Life. *J. Power Sources* **2013**, *231*, 39−43.

(13) Świętosławski, M.; Molenda, M.; Furczoń, K.; Dziembaj, R. Nanocomposite C/Li$_2$MnSiO$_4$ Cathode Material for Lithium Ion Batteries. *J. Power Sources* **2013**, *244*, 510−514.

(14) Ghosh, P.; Mahanty, S.; Basu, R. N. Improved Electrochemical Performance of Li$_2$MnSiO$_4$/C Composite Synthesized by Combustion Technique. *J. Electrochem. Soc.* **2009**, *156*, A677−A681.

(15) Dominko, R.; Bele, M.; Kokalj, A.; Gaberscek, M.; Jamnik, J. Li₂MnSiO₄ as a Potential Li-Battery Cathode Material. *J. Power Sources* **2007**, *174*, 457−461.

(16) Li, Y.-X.; Gong, Z.-L.; Yang, Y. Synthesis and Characterization of Li₂MnSiO₄/C Nanocomposite Cathode Material for Lithium Ion Batteries. *J. Power Sources* **2007**, *174*, 528−532.

(17) Gummow, R. J.; He, Y. Recent Progress in the Development of Li₂MnSiO₄ Cathode Materials. *J. Power Sources* **2014**, *253*, 315−331.

(18) Hu, Z.; Zhang, K.; Gao, H.; Duan, W.; Cheng, F.; Liang, J.; Chen, J. Li₂MnSiO₄@C Nanocomposite as a High-Capacity Cathode Material for Li-Ion Batteries. *J. Mater. Chem. A* **2013**, *1*, 12650−12656.

(19) Wang, F.; Chen, J.; Wang, C.; Yi, B. Fast Sol−Gel Synthesis of Mesoporous Li₂MnSiO₄/C Nanocomposite with Improved Electrochemical Performance for Lithium-Ion Batteries. *J. Electroanal. Chem.* **2013**, *688*, 123−129.

(20) Zhang, S.; Deng, C.; Liu, F. L.; Wu, Q.; Zhang, M.; Meng, F. L.; Gao, H. Impacts of In Situ Carbon Coating on the Structural, Morphological and Electrochemical Characteristics of Li₂MnSiO₄ Prepared by a Citric Acid Assisted Sol−Gel Method. *J. Electroanal. Chem.* **2013**, *689*, 88−95.

(21) Thatshanamoorthy, V.; Suresh, R.; Giribabu, K.; Manigandan, R.; Narayanan, V. Characterization of Mo-MCM-41 and Its Electrochemical Sensing Property. *Synth. React. Inorg., Met.-Org., Nano-Met. Chem.* **2014**, *44*, 1194−1198.

(22) Yang, G.; Deng, Y.; Wang, J. Non-Hydrothermal Synthesis and Characterization of MCM-41 Mesoporous Materials from Iron Ore Tailing. *Ceram. Int.* **2014**, *40*, 7401−7406.

(23) Han, B.; Zhang, F.; Feng, Z.; Liu, S.; Deng, S.; Wang, Y.; Wang, Y. A Designed Mn₂O₃/MCM-41 Nanoporous Composite for Methylene Blue and Rhodamine B Removal with High Efficiency. *Ceram. Int.* **2014**, *40*, 8093−8101.

(24) Xing, Z.; Asiri, A. M.; Obaid, A. Y.; Sun, X.; Ge, X. Carbon Nanofiber-Templated Mesoporous TiO₂ Nanotubes as a High-Capacity Anode Material for Lithium-Ion Batteries. *RSC Adv.* **2014**, *4*, 9061−9063.

(25) Casino, S.; Di Lupo, F.; Francia, C.; Tuel, A.; Bodoardo, S.; Gerbaldi, C. Surfactant-Assisted Sol Gel Preparation of High-Surface Area Mesoporous TiO₂ Nanocrystalline Li-Ion Battery Anodes. *J. Alloys Compd.* **2014**, *594*, 114−121.

(26) Fu, C.; Li, G.; Luo, D.; Huang, X.; Zheng, J.; Li, L. One-step Calcination-Free Synthesis of Multicomponent Spinel Assembled Microspheres for High-Performance Anodes of Li-Ion Batteries: a Case Study of MnCo₂O₄. *ACS Appl. Mater. Interfaces* **2014**, *6*, 2439−2349.

(27) Gregori, M.; Benito, P.; Fornasari, G.; Migani, M.; Millefanti, S.; Ospitali, F.; Albonetti, S. Preparation of Pd/Cu MCM-41 Catalysts for Hydrodechlorination: Influence of the Synthesis Procedure. *Microporous Mesoporous Mater.* **2014**, *190*, 1−9.

(28) Raji, F.; Pakizeh, M. Kinetic and Thermodynamic Studies of Hg(II) Adsorption onto MCM-41 Modified by ZnCl₂. *Appl. Surf. Sci.* **2014**, *301*, 568−575.

(29) Qian, J.; Zhou, M.; Cao, Y.; Ai, X.; Yang, H. Template-Free Hydrothermal Synthesis of Nanoembossed Mesoporous LiFePO₄ Microspheres for High-Performance Lithium-Ion Batteries. *J. Phys. Chem. C* **2010**, *114*, 3477−3482.

(30) Gao, L.; Liu, R.; Hu, H.; Li, G.; Yu, Y. Carbon-Decorated Li₄Ti₅O₁₂/Rutile TiO₂ Mesoporous Microspheres with Nanostructures as High-Performance Anode Materials in Lithium-Ion Batteries. *Nanotechnology* **2014**, *25*, 175402.

(31) Ma, X.; Liu, M.; Gan, L.; Tripathi, P. K.; Zhao, Y.; Zhu, D.; Xu, Z.; Chen, L. Novel Mesoporous Si@C Microspheres as Anodes for Lithium-Ion Batteries. *Phys. Chem. Chem. Phys.* **2014**, *16*, 4135−4142.

(32) Luo, S.; Wang, M.; Sun, W. Fabricated and Improved Electrochemical Properties of Li₂MnSiO₄ Cathodes by Hhydrothermal Reaction for Li-Ion Batteries. *Ceram. Int.* **2012**, *38*, 4325−4329.

(33) Shen, S.; Chen, J.; Koodali, R. T.; Hu, Y.; Xiao, Q.; Zhou, J.; Wang, X.; Guo, L. Activation of MCM-41 Mesoporous Silica by Transition-Metal Incorporation for Photocatalytic Hydrogen Production. *Appl. Catal., B* **2014**, *150−151*, 138−146.

(34) Carraro, P.; Elías, V.; García Blanco, A.; Sapag, K.; Moreno, S.; Oliva, M.; Eimer, G. Synthesis and Multi-Technique Characterization of Nickel Loaded MCM-41 as Potential Hydrogen-Storage Materials. *Microporous Mesoporous Mater.* **2014**, *191*, 103−111.

(35) Gong, H.; Zhu, Y.; Wang, L.; Wei, D.; Liang, J.; Qian, Y. Solid-state Synthesis of Uniform Li₂MnSiO₄/C/Graphene Composites and Their Performance in Lithium-Ion Batteries. *J. Power Sources* **2014**, *246*, 192−197.